ELSEVIER

Chemical Geology 228 (2006) 156–174

CHEMICAL GEOLOGY
INCLUDING
ISOTOPE GEOSCIENCE

www.elsevier.com/locate/chemgeo

Arsenic solid-phase partitioning in reducing sediments of a contaminated wetland

Richard T. Wilkin *, Robert G. Ford

U.S. Environmental Protection Agency, National Risk Management Research Laboratory, Ground Water and Ecosystems Restoration Division, 919 Kerr Research Drive, Ada, Oklahoma 74820, United States

Accepted 6 November 2005

Abstract

The geochemical partitioning of arsenic in organic-rich sediments from a contaminated wetland is examined using X-ray absorption spectroscopy and selective chemical extraction procedures, and evaluated in context to the anoxic diagenesis of iron and sulfur. The interaction between ground water and surface water has a significant influence on iron sulfide formation in the wetland sediments. Ground-water seeps supply concentrations of sulfate, dissolved hydrocarbons, ferrous iron, and arsenic, and sediments located near seeps are anomalously enriched in arsenic, reactive iron, and acid-volatile sulfides. Degree-of-sulfidation (DOS) values are high in sediments adjacent to sites of ground-water discharge, ranging from 0.57 to 1.0. Pyrite (FeS_2) formation is apparently not limited by the abundance of any one primary reactant, e.g., organic carbon, sulfate, or reactive iron; instead, persistence of precursor iron monosulfides is attributed to slow pyrite formation kinetics due to low concentrations of reactive intermediate sulfur species or possibly due to high concentrations of arsenite, dissolved organic-carbon, or other solutes that adsorb to iron monosulfides surfaces and impede transformation reactions to pyrite. Greigite (Fe_3S_4) accounts for >80% of total reduced sulfur in sediments rich in acid-volatile sulfide and X-ray absorption spectroscopy data for magnetic separates provide direct evidence that As(III) is, at least in part, associated with reduced sulfur in the form of greigite. However, pyrite can only account for a small percentage, <20%, of the total arsenic budget in the reduced sediments. Although pyrite is the predicted stable endpoint for reactive iron and sulfur, it appears that within a 30 y time period pyrite is a relatively unimportant host for arsenic in the system investigated here. The abundance of reactive iron in the sediments prevents accumulation of dissolved sulfide and thus prevents formation of soluble thioarsenic species. X-ray absorption near-edge structure (XANES) spectroscopy indicates only the presence of As(III) in the reduced sediments. Results of linear combination fitting of reference spectra to sediment spectra are consistent with sulfur- and/or oxygen-coordinated As(III) in association with iron monosulfides and ferrous-bearing carbonates or hydroxides.
Published by Elsevier B.V.

Keywords: Arsenic; Iron; Pyrite; Greigite; Anoxic sediments; Contaminated sediments; Ground-water/surface-water interactions; XANES spectroscopy; Stable sulfur isotopes

1. Introduction

Complex chemical and physical processes control arsenic concentration profiles in contaminated sediments and adjacent water bodies. Yet predictions about whether arsenic will remain sequestered in the solid

* Corresponding author. Fax: +1 580 436 8703.
E-mail address: wilkin.rick@epa.gov (R.T. Wilkin).

0009-2541/$ - see front matter. Published by Elsevier B.V.
doi:10.1016/j.chemgeo.2005.11.022

phase of sediment matrices or leach into surrounding pore water and overlying water bodies often do not account for this complexity. Model predictions are frequently based solely on examinations of trends in geochemical parameters, such as pH and the oxidation-reduction potential. More complete appraisals of arsenic transport and fate include consideration of microbially mediated redox reactions in sediments involving organic carbon, sulfur, iron, and manganese (e.g., Pierce and Moore, 1982; Aggett and O'Brien, 1985; Edenborn et al., 1986; Brannon and Patrick, 1987; Riedel et al., 1987; Moore et al., 1988; Belzile and Tessier, 1990; Widerlund and Ingri, 1995; Sullivan and Aller, 1996; Kneebone and Hering, 2000; La Force et al., 2000; Mucci et al., 2000; Bose and Sharma, 2002; Chaillou et al., 2003; Nicholas et al., 2003). For instance, oxidized forms of arsenic are often associated with iron oxyhydroxides but can be mobilized via reductive processes, relocalized in the sediment column, and/or diffuse to the overlying water column. Reliable assessments of the biological hazards associated with arsenic from natural and anthropogenic sources depend upon a detailed knowledge of the biogeochemical cycling of this element, in addition to characterization approaches that provide accurate insight into sequestration, transformation, and mobilization processes.

Geochemical relationships among sulfur, iron, and organic carbon in anoxic sediments are primarily governed by the metabolic activity of sulfur bacteria, particularly sulfate-reducing bacteria. These bacteria use dissolved sulfate as the terminal electron acceptor in heterotrophic respiration of organic matter (e.g., Jørgensen, 1982). As bacterial sulfate reduction proceeds, organic carbon is oxidatively consumed and coupled to the reduction of sulfate to sulfide. Biogenic sulfide thus produced can follow a number of pathways (see, e.g., Berner, 1984). A most important pathway with respect to trace metal behavior in sediments is reaction of dissolved sulfide with ferrous iron to precipitate iron sulfides that may be responsible for metal uptake via sorption and/or co-precipitation (e.g., Huerta-Diaz and Morse, 1992; Morse, 1994). The iron disulfide, pyrite, specifically has been viewed as an important carrier of arsenic and other elements (e.g., Raiswell and Plant, 1980; Belzile and Lebel, 1986; Harrison et al., 1991; Kornicker and Morse, 1991; Saunders et al., 1997; Dellwig et al., 2002; Bostick and Fendorf, 2003). Dissolved sulfide can also react directly with arsenic oxyanions (or other trace metals) to form stable complexes, or insoluble precipitates if conditions are favorable, for example, orpiment (As_2S_3) or realgar (As_4S_4). However, a transition from reducing to oxidizing conditions, due either to a shift of predominant redox boundaries or to physical sediment disruption (i.e., dredging, bioturbation), can lead to dissolution of sulfides and potentially arsenic release (Morse, 1994; Saulnier and Mucci, 2000).

Although metal sulfides provide a possible sink for arsenic in anoxic sediments (Moore et al., 1988; Huerta-Diaz et al., 1998; Kneebone and Hering, 2000; Mucci et al., 2000; Dellwig et al., 2002; Chaillou et al., 2003; Bostick et al., 2004), a comparative study suggested that arsenic was less effectively retained in anoxic sediments in Saanich Inlet (British Columbia) relative to equivalent nearby oxic sediments (Peterson and Carpenter, 1983). This observation is noteworthy and likely reflects the overall greater tendency for As(V) oxyanions to bond to mineral surfaces compared to As(III) oxyanions and thioarsenite ions (e.g., Pierce and Moore, 1982). The major mineralogical endpoints of bacterial sulfate reduction are acid-volatile iron monosulfides (mackinawite and greigite) and pyrite. Arsenic adsorption on the surfaces of these phases and/or co-precipitation is thought to be the most important uptake process for metals and metalloids in reducing environments (e.g., Farquhar et al., 2002; Wolthers et al., 2005a). Yet there is scant evidence showing an association between arsenic and iron monosulfide phases. In contrast, more conclusive data show the occurrence of arsenic in pyrite (arsenian pyrite). The concentration of arsenic in various textural forms of pyrite, including euhedral grains and framboids, ranges from ~0 to approximately 10 wt.% (e.g., Ostwald and England, 1979; Jacobs et al., 1985; Vavelidis, 1995; Graham and Robertson, 1995; Kolker et al., 1998). Recent molecular studies indicate that arsenic substitutes for sulfur in pyrite (FeS_2) as a solid solution (Savage et al., 2000). This finding has environmental significance because pyrite is highly insoluble over a range of geochemical conditions; consequently, pyrite is potentially a stable host in reducing environments for contaminants such as arsenic. Limited field and laboratory evidence suggests that rates of pyritization in natural systems may be quite variable and dependent on several key factors that include, for example, pH, redox conditions, and concentrations of reactive species and reaction inhibitors (e.g., Rickard et al., 1995; Gagnon et al., 1995; Hurtgen et al., 1999; Morse, 1999).

The objective of this study is to characterize, using an array of analytical methods, the distribution and associations of arsenic in contaminated, anoxic wetland sediments that were deposited in an urban watershed. Of particular interest is the development of an improved understanding about the relationships between arsenic cycling and the diagenetic behaviors of iron and sulfur

and their general implications to the long-term stability of arsenic in anoxic sediments. The site investigated in this study is a constructed pond (Hall's Brook Holding Area) located adjacent to a hazardous waste site (Industri-Plex Superfund site). The pond receives arsenic, in addition to elevated concentrations of dissolved hydrocarbons, ferrous iron, and sulfate, primarily through ground water seeps. A more detailed site description and history is presented within a companion publication in this volume (Ford et al., 2006-this volume).

2. Methods

2.1. Sample collection and preparation

Sediment samples were collected in December 1999, April 2001, and September 2001 from the Hall's Brook Holding Area (HBHA) pond. The site is located near Woburn, Massachusetts, approximately 16 km northwest of downtown Boston (Fig. 1). Outflow from the pond feeds into the Aberjona River approximately 1 km downstream of the site and eventually into Upper Mystic Lake. The greatest density of sampling points is along the center axis and along the northeast shore of the pond, where contaminated ground water discharges into the pond. Sediment samples were retrieved from water depths ranging from 0.5 to 4.5 m. Cores were collected using a 5-cm diameter piston-coring device. The cores were capped immediately after their recovery and kept upright before and during freezing. Surface sediments were collected into N_2-purged plastic bags by pumping highly fluidized sediments to the surface using a peristaltic pump. Surface sediments and cores were frozen within 1 h of collection from the pond bottom. While still frozen, sediment cores were sub-sampled by cutting off 2- to 5-cm thick sections, which were immediately bagged and kept frozen for subsequent solid-phase analyses. In the laboratory, sediments were thawed and dried at room temperature in an anaerobic glove box (96 : 4 v/v N_2–H_2 gas mixture). Excess pore water was squeezed from the sediments and decanted during the drying process. Dried samples were homogenized with an agate mortar and pestle and retained in the anaerobic glove box. Sample splits were removed from the glove box and allowed to oxidize in an oven at 50 °C for 72 h.

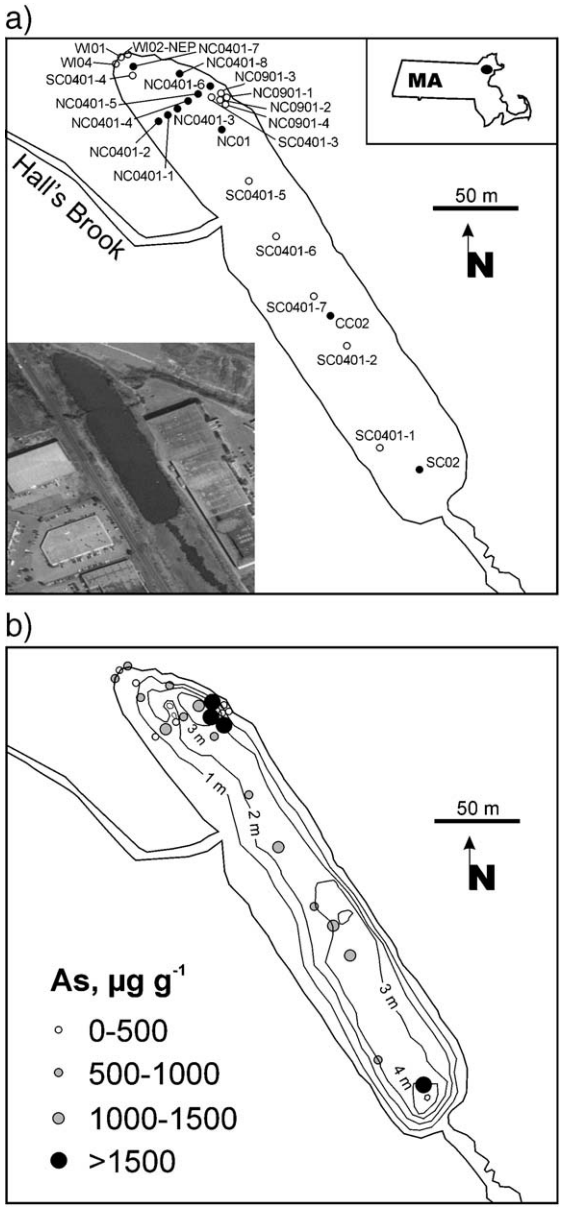

Fig. 1. Map of the study area showing a) the location of sampling locations (cores = filled circles; surface sediments = open circles) and inset aerial photograph of the HBHA pond, and b) sediment depth contours and the arsenic concentration distribution in surface sediments.

2.2. Solid-phase characterization

Methods used for solid-phase characterization are listed in Appendix A.1 along with method detection limits, and analytical accuracy and precision. All solid-phase concentrations are reported on a dry weight basis. Total carbon and carbonate carbon were determined on oven-dried samples using a UIC (Model CM5014) carbon coulometer system (Huffman, 1977). Organic carbon content was derived from the difference between total carbon and inorganic carbon. For total carbon

analysis, 20–300 mg of powdered sediment was combusted at 950 °C. Inorganic carbon was analyzed as carbon dioxide released from a sample after reaction with hot 5% perchloric acid.

Total sulfur was determined by mixing oven-dried sediment samples with vanadium pentoxide and combusting the mixture in the presence of high-purity oxygen-gas at 1050 °C (Atkin and Somerfield, 1994). Sulfur dioxide produced is quantitatively titrated using a sulfur coulometer (UIC Model CM5014S). Sediment concentrations of acid-volatile sulfide (AVS) and chromium-reducible sulfur (CRS) were determined using sequential chemical extraction methods (Chanton and Martens, 1985; Canfield et al., 1986; Tuttle et al., 1986). AVS was determined by reacting 300 to 700 mg of sediment dried in a glove box (unoxidized sediments) with 10 mL of boiling 1 M HCl containing 10% by weight of $SnCl_2$. Stannous chloride prevents the possible oxidation of hydrogen sulfide by ferric iron. Evolved hydrogen sulfide gas was flushed via an N_2 carrier gas and titrated using the sulfur coulometer or trapped in a deoxygenated solution of 0.1 M $AgNO_3$. The resulting sulfide precipitate was rinsed with boiling water, dried, and weighed for gravimetric determination as Ag_2S. Hydrogen sulfide gas evolved from samples after reaction with boiling 1 M $CrCl_2$ in 0.5 M HCl (mainly from pyrite) was coulometrically titrated or trapped as silver sulfide and used for sulfur isotope analyses. The quantities of AVS–iron and pyrite–iron are calculated from the sulfur extraction results assuming stoichiometries of FeS and FeS_2, respectively. Sulfate–sulfur was determined by extracting unoxidized sediments with N_2-purged, 2.3 mM $NaHCO_3$/2.4 mM Na_2CO_3 buffer solution for 24 h in an anaerobic glove box. Extractant solutions were filtered using 0.22-μm syringe filters (cellulose acetate) and analyzed for sulfate by capillary electrophoresis (Waters CE).

Sulfur isotope compositions of CRS for a selection of core samples were determined from Ag_2S precipitates at the Environmental Isotope Laboratory (University of Waterloo, Waterloo, Ontario) using isotope ratio mass spectrometry. Sulfur isotope compositions of water-column sulfate were determined from $BaSO_4$ precipitates. Sulfur isotope data are reported using the $\delta^{34}S$ notation as permil deviations from the stable sulfur isotope composition of the Cañon Diablo troilite standard. Precision of sulfur isotope determinations (±0.2‰) was estimated based on repeated measurements of Ag_2S precipitated from a laboratory-prepared Na_2S solution.

Concentrations of metals and metalloids in the sediments were determined by microwave assisted digestion in 10% HNO_3 (modified EPA Method 3051), followed by inductively coupled plasma optical emission spectrometry (ICP-OES, Perkin Elmer Optima 3300DV). Microwave digestion was carried out using a CEM Mars 5 system at a total pressure of 120 psi (8.5 bar) and maximum temperature of 170 °C. The reliability of this digestion method was continuously checked using international certified reference materials (NIST 2710, NIST 2780, and CCRMP LKSD-1). Arsenic recovery from these reference materials, for example, ranged from 88% to 97% of the certified values.

A series of single-step chemical extractions were performed to better constrain the solid-phase partitioning of arsenic. All solutions were deoxygenated prior to use and extractions were carried out using unoxidized sediments in an anaerobic glove box. The following solutions were used: 1 M $MgCl_2$, 0.1 M Na_2CO_3, and 1 M HCl. Dilute hydrochloric acid extractions were conducted on both unoxidized and oxidized sediment samples. Supernatant solutions were filtered through 0.22-μm syringe filters and acidified with concentrated nitric acid. The analysis of metals in the solutions obtained following chemical extraction was carried out using ICP-OES.

For selected samples retained in the anaerobic glove box, magnetic fractions were collected using a hand magnet. The mineralogy of selected bulk sediments and magnetic fractions was investigated using powder X-ray diffraction (Rigaku Miniflex) with Fe–Kα radiation (5–90° 2θ, 0.2° step interval at 0.02° per minute scan speed).

2.3. XANES analysis

The oxidation state and bonding environment of arsenic associated with the sediments was examined using X-ray absorption near edge structure (XANES) spectroscopy. Arsenic K-edge spectra were collected at beamline 20-BM (PNC Collaborative Access Team) and 5-BM (DND Collaborative Access Team) at the Advanced Photon Source, Argonne National Laboratory (Argonne, IL). Sediment samples were loaded into 1.5-mm-thick plastic sample holders and sealed with strips of Kapton tape. All sample and mineral reference solids were handled in a N_2-filled glove bag to minimize oxidation of arsenic and other redox-sensitive elements. Absorption spectra were collected at the As edge (11,867 eV) in fluorescence mode using a 13-element solid-state Ge-detector. The synchrotron was operated at 7.0 GeV and at a nominal 100 mA fill current. The energy of a Si(111) double-crystal monochromator was

calibrated using arsenic or gold foil. The monochromator step size was 0.25 eV per step in the XANES region (11,830–11,900 eV). Multiple scans were collected and summed for each sample (3 to 9). The XANES fluorescence data were normalized to the edge-jump height and the K-edge inflection point was determined as the energy at the maximum in the first derivative of the normalized spectra. All fluorescence spectra were collected at room temperature.

Mineral reference compounds were purchased from Wards Scientific (arsenopyrite, realgar) or synthesized in the laboratory (mackinawite, pyrite, orpiment, siderite, carbonate green rust) in systems containing arsenite following procedures outlined in Wilkin and Barnes (1996), Wilkin and Ford (2002), and Su and Wilkin (2005). Arsenopyrite, realgar, and orpiment were diluted with inert boron nitride so that the resulting bulk arsenic concentration was near 0.5 wt.%. Linear combination fitting of XANES data was carried out using the WinXAS software package version 3.1 (Ressler, 1998). Normalized XANES spectra of reference compounds were combined and fit using a least-squares procedure to unknown samples over an energy range from 11,830 to 11,890 eV. During linear combination fitting, energy shift adjustments of the reference spectra were not allowed to exceed 0.50 eV and reference compounds returned with negative concentrations were omitted from the fitting analysis.

2.4. Surface- and pore-water characterization

Surface waters and sediment pore waters were collected using membrane diffusion samplers and tubing wells installed using Geoprobe® equipment. Discrete multi-level samplers (DMLS; Ronen et al., 1987), constructed from stainless steel, were deployed to collect 15 ml of sediment pore-water at approximately 5 cm intervals. Using these samplers, pore water was collected to a depth of about 1 m below the sediment–water interface and pond bottom-water was collected from regions immediately superjacent to the sediment–water interface. Tubing wells equipped with 6-in. stainless steel screens were placed by driving a 1-in. rod, rigged with an expendable tip holder, to the desired depth with an electric hammer. A semi-permanent sampling station (NML) was constructed by attaching 6-in. screens to PVC pipe at 0.5 m intervals. The PVC pipe was anchored into the sediments and tubing from each sampling screen, placed above and below the sediment–water interface, was extended to the shoreline and secured for repeated use. Water samples were taken directly from the DMLS units or were collected from tubing well installations using a peristaltic pump. Water samples for metals analysis by ICP-OES were filtered through a 0.45-μm filter (cellulose nitrate membrane) and acidified to pH<2 by adding concentrated nitric acid (Optima). Samples for anionic species were treated similarly but were not acidified. All water samples were stored in a refrigerator until analysis was completed.

3. Results and discussion

3.1. Arsenic distribution in sediments

Below a water depth of 1.5 to 2 m in the HBHA pond, surface sediments consist of black-colored, gelatinous, organic carbon-rich mud overlying tan- to gray-colored, medium- to coarse-grained sand. The contact between these two sediment types is sharp and the lower sandy unit likely represents the original liner of the constructed pond (Davis et al., 1996). The recovered thickness of black sediments in cores ranged from 10 to 30 cm, which corresponds to a net sedimentation rate of about 0.4 to 1.2 cm y^{-1} assuming no compaction, since the pond was constructed in 1974. Sediments at the sediment–water column interface are notably very fine-grained and easily re-suspended.

Concentrations of total arsenic in surface sediments (0–4 cm) from the HBHA pond range from about 20 to 2100 μg g^{-1} (Fig. 1b). The highest sediment concentrations of arsenic tend to be present in the northeast corner of the pond. Yet arsenic concentrations as high as 1570 μg g^{-1} (SC02) are found in sediments near the southern end of the pond, at depths below 3 m. Ground water seeps along the northeastern shore are considered to be the primary sources of arsenic to the pond (Davis et al., 1996; Ford et al., 2006-this volume), so the even concentration distribution of arsenic along the center axis suggests that sediment reworking during high-flow events and possibly chemical cycling between the water column and sediments are important processes that govern the distribution of arsenic and other metals in the HBHA pond. Alternatively, it is possible that other unidentified sources of arsenic to the pond exist, although this is considered to be unlikely based on systematic ground-water surveys in areas adjacent to the pond.

Depth-dependent, sediment concentration distributions (dry weight) of carbon, sulfur, iron, and arsenic are shown in Fig. 2 for cores NC01 and SC02. In both cores, arsenic concentrations are uniform at depths above 10 cm in the sediment column. Below a depth of about 10 cm, arsenic concentrations abruptly decrease with increasing depth. In cores NC0401-3, NC0401-4,

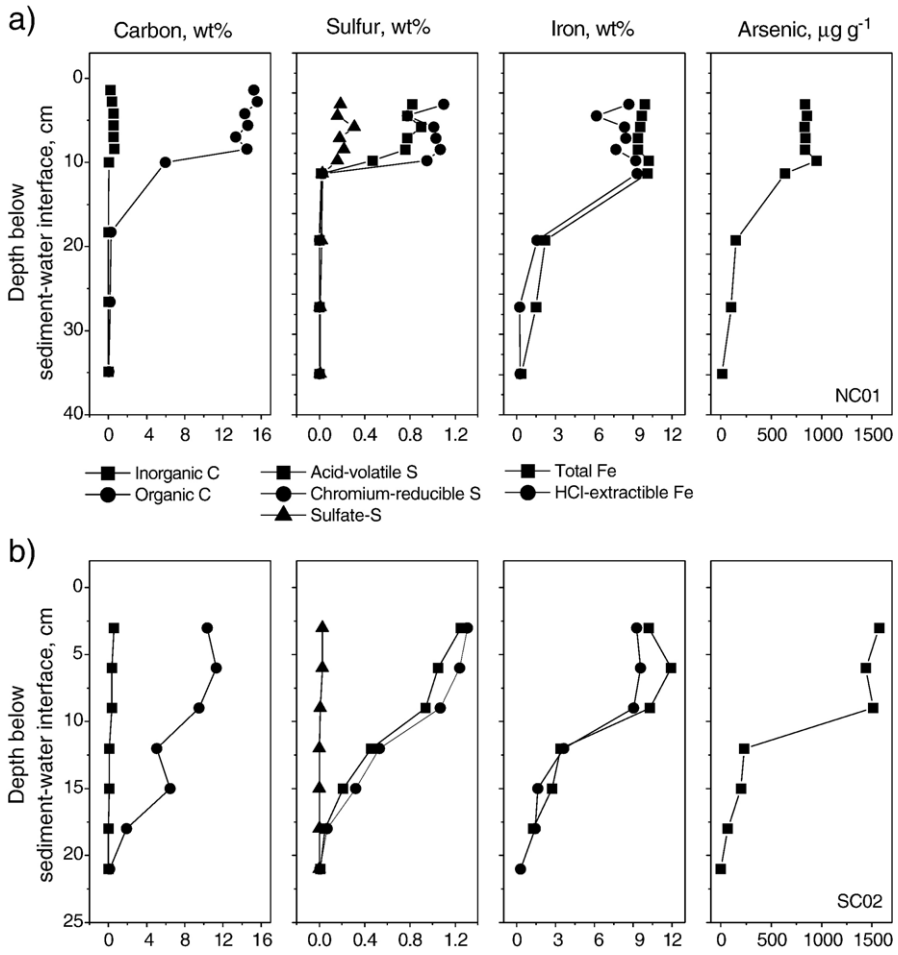

Fig. 2. Concentration profiles vs. depth for carbon (wt.%), sulfur (wt.%), iron (wt.%), and arsenic (µg g^{-1}) in HBHA cores: a) NC01 and b) SC02.

NC0401-5, and NC0401-6, arsenic shows a subsurface peak in the depth range from approximately 5 to 10 cm below the sediment–water interface (data not shown). In these cores, the depletion of arsenic in the surface sediments may be coupled to arsenic release to the overlying water column.

Arsenic clearly shares similar concentration distributions with organic carbon, sulfur, and iron (Fig. 2). Statistical correlations of elemental abundance with arsenic and other selected elements are presented in Table 1 for the complete data set ($n=76$), including cores and surface sediments. Arsenic abundance has a high degree of positive correlation ($r>0.7$) with iron, cadmium, sulfur, calcium, zinc, vanadium, organic carbon, and sodium. Of these elements, significant average molar ratios with arsenic are noted for organic carbon (702), iron (123), sulfur (68), and calcium (23), although molar ratios in any given sample can vary widely. Thus, analysis of arsenic concentration trends and correlation with other abundant elements are suggestive that diagenetic cycling of iron, carbon, and/or sulfur controls the solid-phase distribution of arsenic (e.g., Aggett and O'Brien, 1985; Sullivan and Aller, 1996; Loring et al., 1998; Chaillou et al., 2003). Nevertheless, these relationships are inconclusive in the absence of other supporting data, such as mineralogical characterization, selective chemical extractions, and/or spectroscopic analyses.

3.2. Pore-water arsenic

Maximum dissolved arsenic concentrations up to about 2 mg l^{-1} occur near the sediment–water interface (Fig. 3). Pore-water and bottom-water concentration profiles are consistent with both upward and downward diffusion of arsenic from the sediment–water interface. Dissolved arsenic profiles closely follow the patterns of total dissolved iron and sulfate (Fig. 3). Decreasing

Table 1
Statistical correlations of total element concentrations with arsenic, total organic carbon (TOC), iron, and sulfur in the HBHA pond sediments

Element	As	TOC	Fe	S
As	1	0.73	0.86	0.83
TOC	0.73	1	0.84	0.43
Fe	0.86	0.84	1	0.59
S	0.83	0.43	0.59	1
TIC	0.56	0.74	0.70	0.31
Al	0.66	0.68	0.72	0.45
Mn	0.57	0.85	0.83	0.16
Cd	0.86	0.69	0.80	0.79
Pb	0.27	0.43	0.37	0.14
Zn	0.82	0.55	0.77	0.84
Cu	0.66	0.71	0.68	0.51
Co	0.31	0.05	0.24	0.53
Ni	0.58	0.27	0.47	0.74
Cr	0.62	0.89	0.82	0.30
V	0.76	0.88	0.84	0.44
Mg	0.50	0.57	0.54	0.29
Ca	0.82	0.90	0.86	0.59
Na	0.72	0.57	0.59	0.68
K	0.59	0.64	0.65	0.32

TIC is total inorganic carbon. Correlation matrix determined from complete data set, including cores and surface sediments ($n=76$). All sediments are from depths below 1 m.

arsenic concentrations above the sediment–water interface are related to iron and arsenic oxidation in the water column, and arsenic uptake onto hydrous ferric oxide precipitates (Ford et al., 2006-this volume). Decreasing arsenic concentrations with depth below the sediment–water interface suggests removal of arsenic from pore water into sediment due to scavenging by mineral or organic substrates.

Although the bottom-water and pore-water profiles shown in Fig. 3 indicate that the HBHA pond sediments are a sink for dissolved arsenic, the sediments also appear to be a source of dissolved arsenic to the overlying water column. Arsenic, released from the sediments and accumulated in bottom waters, could be flushed out of the HBHA pond and transported to regions hydraulically downgradient of the pond, for example, during anomalous precipitation and high-flow events. In the absence of sediment disturbances from bioturbation or from advective transport, molecular diffusion fluxes calculated from pore-water data should provide a reasonable estimate of instantaneous arsenic release from sediments to bottom waters. Vertical diffusion fluxes of arsenic were estimated using Fick's First Law, concentration gradients, ion diffusion coefficients corrected for sediment tortuosity, and sediment porosity of 0.95 (Li and Gregory, 1974; Berner, 1980). Li and Gregory (1974) provide a diffusion coefficient for the singly deprotonated arsenate anion ($As(OH)_2O_2^-$) of 9.05×10^{-6} cm^2 s^{-1} at 25 °C. For the estimates made here, we assume that this value is appropriate for both arsenate and arsenite and for a range of temperatures from approximately 10 to 20 °C.

Upward arsenic fluxes range from 0.07 to 0.15 μmol cm^{-2} y^{-1} and are comparable to downward directed arsenic fluxes, 0.10 to 0.22 μmol cm^{-2} y^{-1}. The values reported here for pore-water production fluxes are higher compared to those reported in previous investigations of estuarine and coastal marine environments (e.g., Widerlund and Ingri, 1995; Sullivan and Aller, 1996; Chaillou et al., 2003). Higher production fluxes in this study are likely related to higher sediment concentrations of arsenic and other site-specific geochemical conditions, e.g., high DOC concentrations and redox conditions. Assuming that arsenic production is constant at depths below 1 m (~12,000 m^2), HBHA pond sediments could release 0.6 to 1.3 kg of arsenic per year, although we suspect that this mass range is an upper estimate based on the location of the pore-water and surface-water assessments and based on arsenic concentration distributions in sediments and pore waters from other regions of the HBHA pond. Arsenic released to the water column is effectively taken up by hydrous ferric oxide particles in the water column (Ford et al., 2006-this volume). Following a similar analysis of instantaneous iron fluxes, HBHA pond sediments could release up to 54 kg of iron per year. Evident from Fig. 3 is that arsenic removal from sediment pore waters is accompanied by removal of iron and sulfate (sulfate reduction) as discussed in following sections.

3.3. Pyrite formation

Concentration profiles of solid-phase forms of sulfur show enrichments in the organic-rich mud and clear decreasing trends with depth towards the underlying sand liner (Fig. 2). The major forms of sulfur present are chromium-reducible sulfur (mainly pyrite plus elemental sulfur, 0–82% of total sulfur), acid-volatile sulfides (mainly iron monosulfides, 0–90% of total sulfur), and sulfate–sulfur (soluble/desorbed sulfate and sulfate from residual pore water, 0–18% of total sulfur). Other forms of solid-phase sulfur, such as organic sulfur, may be present but only in minor amounts because in all cases the sum of CRS+AVS+sulfate–sulfur accounts for >90% of the total concentration of sulfur in samples with >0.1 wt.% S.

The sulfur isotope composition of pyrite–sulfur (CRS) is shown in Fig. 4 for cores NC01 and SC02.

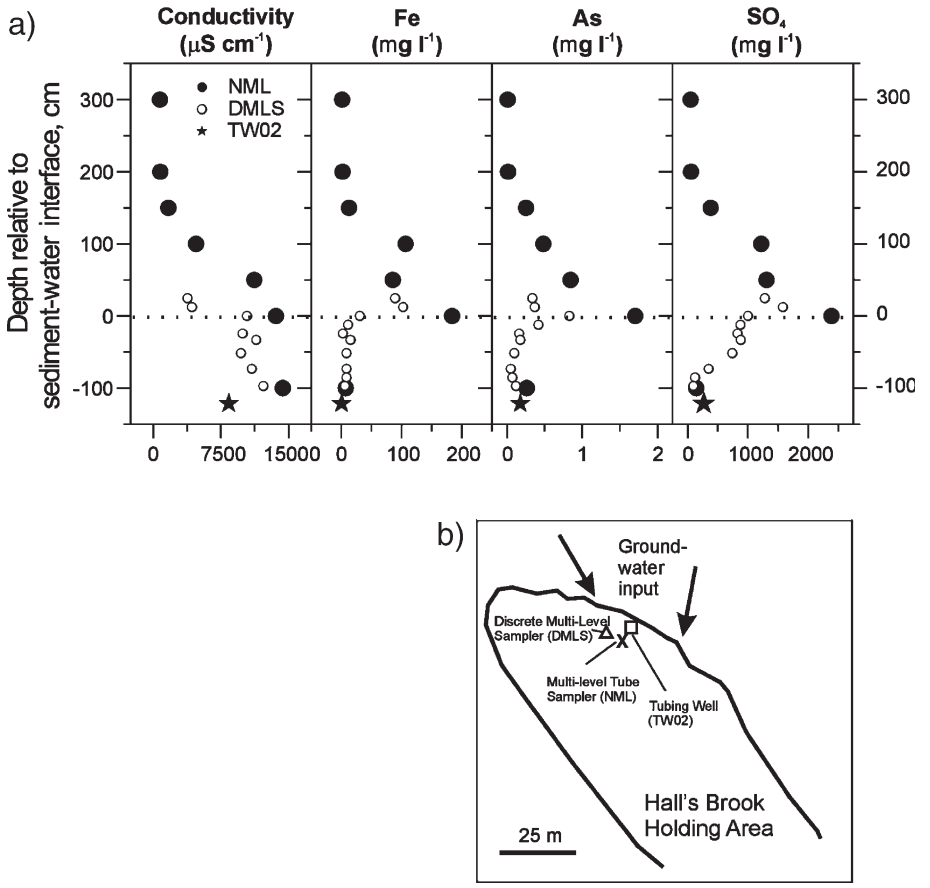

Fig. 3. Pore-water and surface-water profiles of a) conductivity, iron, arsenic, and sulfate at distances relative to the sediment–water interface, and b) map showing location of diffusion samplers and tubing wells discussed in text.

The majority of solid-phase sulfur appears to be fixed at or near the sediment–water interface because the total sulfur concentration, distribution of sulfur forms, and their sulfur isotope compositions are broadly consistent throughout the allochthonous mud. The difference between the average sulfur isotopic composition of pyrite–sulfur and water-column sulfate (+10.14 ±0.11‰, $n=2$), the apparent isotope fractionation, varies from 37.6‰ to 29.0‰. This range of $\Delta\delta^{34}S$ values is fairly typical for freshwater and marine systems. The smaller degrees of isotopic fractionation in core SC02 could be due to the sulfate concentration effect (Canfield, 2001). Sulfate concentrations in the bottom waters of the pond near the location of SC02 are <6.0 mM compared to the higher sulfate concentrations of up to 18.5 mM in bottom water near NC01. Laboratory evidence suggests that sulfur isotope fractionation during sulfate reduction decreases with sulfate concentrations (McCready, 1975; Chambers and Trudinger, 1979; Canfield, 2001). The gradient in bottom water sulfate concentrations is caused by the

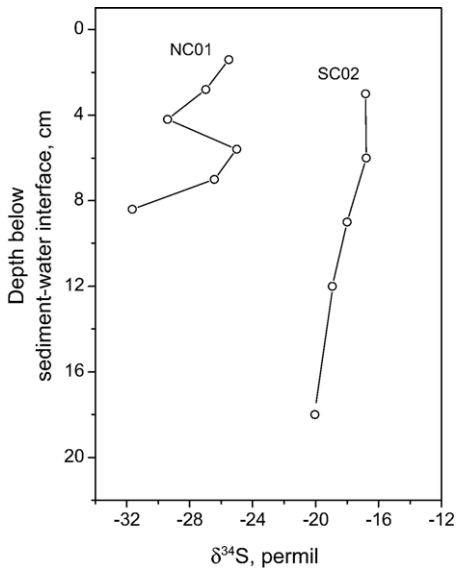

Fig. 4. Depth profile of $\delta^{34}S$ values for pyrite in HBHA cores NC01 and SC02.

focused discharge of ground water enriched in sulfate as well as arsenic, dissolved hydrocarbons, and ferrous iron in the vicinity of NC01.

Reactive iron is strikingly abundant in the HBHA pond sediments. Solid-phase iron is partitioned into three major forms: pyrite–iron (Fe_{pyr}), acid-volatile sulfide–iron (Fe_{AVS}), and non-sulfidized reactive-iron ($Fe_{reac}=Fe_{HCl}-Fe_{AVS}$). Other iron fractions include total iron (Fe_T), iron leached with 1 M HCl (Fe_{HCl}), and total reactive iron ($Fe_{pyr}+Fe_{HCl}$). In most samples, the major iron form is Fe_{reac}. The average quantity of sulfidized iron ($Fe_{pyr}+Fe_{AVS}$) in the sediments is only about 34% of Fe_T ($n=42$), although as discussed below the degree of iron sulfidation varies spatially in the pond. Concentrations of total reactive iron range from ~0.5 to 18 wt.% (average=7.6 wt.%) and are in excellent agreement with Fe_T values ($r=0.95$; $n=45$). The detailed speciation of non-sulfidized iron in these sediments has not been determined and this is an area that requires more assessment. However, the non-sulfidized iron fraction is likely associated with a range of carbonate, hydroxide, oxyhydroxide, and/or organic components.

The relationship between total sulfur and total reactive iron is shown in Fig. 5. In this figure, lines are drawn for the expected relationship if all sulfur is present as the iron sulfides: mackinawite (FeS), greigite (Fe_3S_4), and pyrite (FeS_2), and all iron is present in a sulfide form. The majority of samples (filled circles) plot in a region above the FeS line, indicating that these samples have excess reactive iron over sulfur, i.e., the formation of iron sulfides in these samples is not limited by reactive iron. The data trend shown with open circles

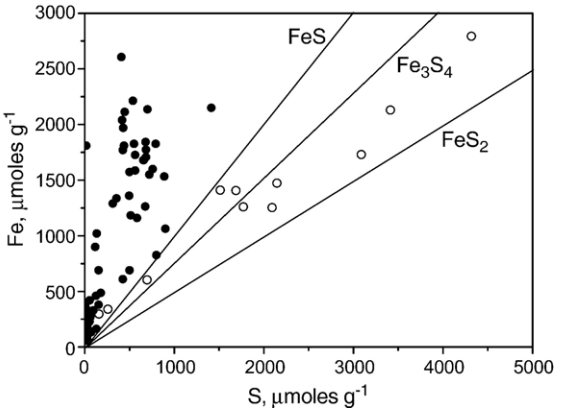

Fig. 5. The relationship between total sulfur and total reactive iron in HBHA pond sediments. Lines indicate the trends expected if all iron and sulfur were present as FeS, Fe_3S_4, or FeS_2. Filled- and open-circles, respectively, represent sediment samples distally located and adjacent to ground-water seeps (see text).

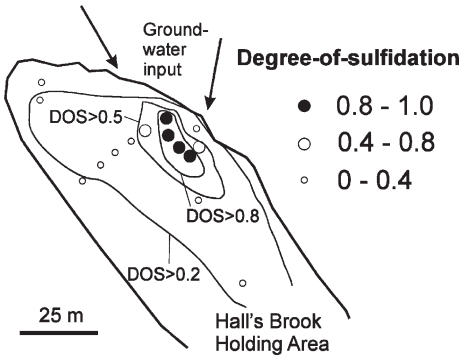

Fig. 6. Map showing distribution of degree-of-sulfidation (DOS) values in the northern half of the HBHA pond. Note that anomalous DOS values (>0.8) are concentrated in a region where contaminated ground water discharges into the pond.

in Fig. 5 represents samples spatially restricted to a region along the northeastern shore of the pond, where the predominant ground-water seeps are located. Note that these samples are comparatively enriched in sulfur and contain Fe/S ratios consistent with a mixture of FeS_2, Fe_3S_4, and FeS, i.e., in these samples reactive iron is nearly completely sulfidized.

Boesen and Postma (1988) introduced the degree-of-sulfidation (DOS), which is calculated as:

$$\mathrm{DOS} = \frac{Fe_{AVS} + Fe_{pyr}}{Fe_{pyr} + Fe_{HCl}}$$

DOS is a common measure of the extent to which reactive iron has been sulfidized to form pyrite and/or acid-volatile iron monosulfides. DOS values are low in sediments distally located from the ground-water seeps (0.17 ± 0.10, $n=35$), even though total sulfur values in these sediments are comparatively high for freshwater systems, up to 2.85 wt.%. Low DOS values are an indication that availability of reactive iron is not a limiting control on the formation of iron sulfides. In contrast, DOS values are very high in surface sediments proximal to the ground-water seeps along the northeastern shore of the pond (0.80 ± 0.24, $n=10$; Fig. 6), and total sulfur values are anomalously high, up to 10.95 wt.% (in SC0401-3). The high DOS values in samples from this region of the pond likely stem from their immediacy to a ground-water source of highly metabolizable organic carbon (DOC concentrations exceeding 50 mM) and high concentrations of sulfate (up to approximately 18.5 mM). These features are consistent with the observed $\Delta\delta^{34}S$ values of chromium-reducible sulfur in core NC01 as compared to core SC02 because the larger isotope shift in core NC01 is suggestive of higher sulfate concentrations and/or more labile organic matter.

The high DOC concentrations encountered in the HBHA pond sediments, bottom waters, and sediment pore waters are derived from several natural and anthropogenic sources, including sources that stem to waste management practices dating back approximately 100 y. The nature and reactivity of some of the dissolved organic carbon compounds at this site were discussed by Wick and Gschwend (1998) and Wick et al. (2000). A range of compounds, including benzene, phenols, and sulfonates, were identified in these studies that could be linked back to specific industrial processes. In sum, however, these compounds still only make up a small fraction of the total DOC pool.

In sediments near the ground water seeps, reactive iron is effectively sulfidized but not necessarily converted to pyrite. In these sediments, AVS–sulfur: FeS_2–sulfur ratios are typically greater than 1 (0.19 to 16.4; average 3.17, $n=10$). Sediments more distal to the ground water seeps have lower AVS–sulfur: FeS_2–sulfur ratios (0.63 ± 0.35, $n=32$), but are still comparatively enriched in AVS–sulfur (see Gagnon et al., 1995, their Table 2). The extent of conversion from AVS to pyrite is significant in this study because contaminant species such as arsenic that might be associated with AVS phases are potentially mobile due to the susceptibility of iron monosulfides to oxidize and/or to dissolve. On the other hand, pyrite is considerably more stable, less soluble, and less readily oxidized compared to mackinawite and greigite. High AVS–sulfur: FeS_2–sulfur ratios suggest that the transformation reaction from iron monosulfides to pyrite is either incomplete after the <30 y of sediment deposition represented in the core samples, or the transformation reaction is inhibited from going to completion. Inhibition of pyrite formation could be due to limited availability of reactive intermediate sulfur species or other oxidants necessary to drive the iron monosulfide-to-pyrite transformation (e.g., Boesen and Postma, 1988; Middelburg, 1991; Gagnon et al., 1995; Hurtgen et al., 1999). Morse (1999) has recently suggested that high DOC concentrations (1–4 mM) in the sediments of the Laguna Madre (Texas, USA) could be responsible for low rates of pyritization in those sediments. Much higher concentrations of DOC (up to 50 mM), related to a dissolved hydrocarbon plume that discharges into the HBHA pond, are present in this study and could be partly responsible for both anomalous sulfidation and inhibition of iron sulfide transformation reactions. Finally, an especially intriguing mechanism of inhibition is possible based on recent laboratory experiments (Wolthers et al., 2005b). This study showed that As(III) was effective in slowing the transformation of FeS to pyrite, perhaps due to stabilization of the FeS precursor surface. It is interesting to note that sediments with the highest AVS–sulfur: FeS_2–sulfur ratios also tend to have the highest concentrations of arsenic so that arsenic could play a role in retarding the rate of pyritization.

Table 2
Arsenic K-edge positions and concentrations of total sulfur, iron, and arsenic for selected HBHA pond sediments, <2 mm size fraction for WI01, WI02-NEP, and WI04

Sample	Water depth, m	S_T, wt.%	Fe_T, wt.%	As_T, μg g^{-1}	As K-edge, eV
WI01	<0.5	0.20	3.8	494	11,873.2/11,869.8
WI02-NEP	<0.5	0.65	18.5	630	11,873.7/11,869.7
WI04	<0.5	0.35	26.3	840	11,873.2/11,869.2
NC0901-1	1.0	0.83	1.90	163	11,873.5/11,869.7
SC0401-1	2.1	1.14	7.46	531	11,868.2
SC0401-6	2.6	2.85	8.56	1028	11,868.0
SC0401-7	3.1	2.32	8.65	1039	11,868.7
SC0401-3	3.2	10.95	11.9	1780	11,867.9
NC0901-4b	3.5	5.68	7.04	1275	11,868.7
NC0901-4c	3.5	6.89	8.23	1213	11,868.3

Despite active sulfate-reduction indicated by the buildup of solid-phase reduced sulfur compounds in HBHA pond sediments, concentrations of dissolved sulfide in bottom waters of the pond were never detected ($\sum H_2S<1$ μm). Low sulfide concentrations are likely maintained by rapid precipitation of iron monosulfides in the presence of abundant dissolved Fe(II) and reducible solid-phase Fe(III) (e.g., Canfield, 1989). It is unlikely that H_2S is directly involved in pyrite formation reactions because dissolution of reactive iron minerals is apparently greater than the net rate of sulfide production in the sediments. The excess of reactive iron over sulfide is significant in the context of controlling arsenic speciation in that the formation of soluble and generally mobile thioarsenic species is prevented in systems with abundant reactive iron (Wilkin et al., 2003). Speciation of arsenic in the aqueous phase, primarily as the oxyanions arsenite and arsenate, should play an important role in directing sorption and co-precipitation reactions (e.g., Ford et al., 2006-this volume).

Magnetic materials were separated from sediment samples SC0401-3 and NC0901-4b; these samples contain high concentrations of total sulfur, 10.95 and 5.68 wt.%, respectively. Powder X-ray diffraction results for sample SC0401-3 are shown in Fig. 7. The X-ray spectrum for SC0401-3 indicates the presence mainly of quartz and greigite. Greigite is a ferrimagnetic thiospinel and probably represents a transformation product from mackinawite (e.g., Schoonen and Barnes, 1991; Lennie et al., 1997). Mass balance indicates that

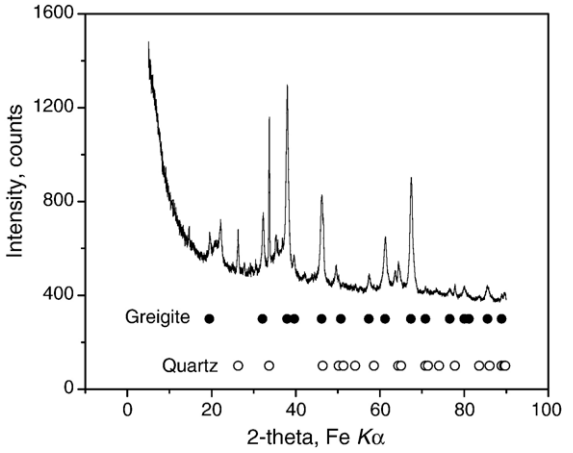

Fig. 7. X-ray diffraction pattern of surface sediment SC0401-3 showing the presence of greigite (PDF Card No. 16-0713) and quartz (PDF Card No. 46-1045).

greigite represents >80% of total reduced sulfur in SC0401-3 and NC0901-4b. Rickard et al. (2001) recently concluded that the presence of organic carbon compounds during iron sulfide precipitation and transformation play a role in controlling mineralogical endpoints. Greigite was found to be the dominant endpoint, instead of pyrite, in systems containing aldehydic carbonyls. The notable abundance of greigite in HBHA pond sediments may be related to the abundance of organic carbon compounds, both from the previously discussed kinetic perspective (Morse, 1999) and from a mineral crystallization perspective (Rickard et al., 2001).

3.4. XANES analysis

X-ray absorption near-edge structure (XANES) spectroscopy is used here to probe possible solid-phase associations of arsenic by comparing spectra of known arsenic-bearing reference materials with spectra of unknown samples collected from the HBHA pond. The arsenic K-edge spectra and their first derivatives for As(III) reference materials are shown in Fig. 8. The individual reference materials are arranged to show a subtle energy shift of the arsenic absorption edge position from 11,866.3 eV for arsenopyrite to 11,869.0 eV for As(III) associated with siderite, a total shift of 2.7 eV. Note that siderite, carbonate green rust, mackinawite, pyrite, and precipitated orpiment were all prepared in the laboratory using sodium arsenite as the arsenic source. Arsenopyrite and realgar are from natural sources.

The first derivative data (Fig. 8b) indicate different structural and/or electronic environments around arsenic in the synthetic and natural reference minerals. It is unlikely that these spectra are uniquely diagnostic because not all possible arsenic associations have been included in the selection of reference materials, e.g., arsenite associated with organic carbon. In general, the absorption edge shifts to higher energy with increasing As oxidation state. However, because all of the reference materials plotted in Fig. 8 contain arsenic present in the +3 oxidation state, with the exception of arsenopyrite in which the formal oxidation state of arsenic is −1 (Simon et al., 1999; Jones and Nesbitt, 2002), the subtle energy shift of the absorption edge

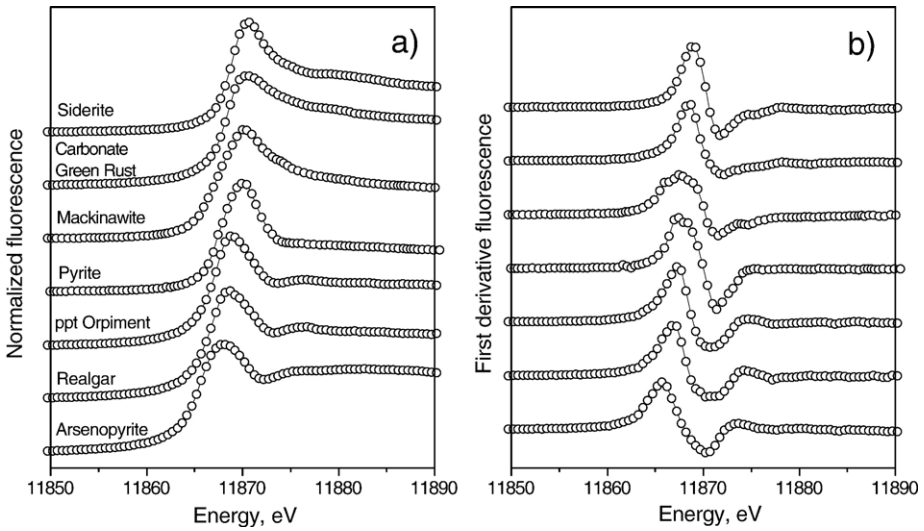

Fig. 8. a) Arsenic K-edge XANES spectra, and b) first derivative spectra for reference materials: arsenopyrite, realgar, precipitated orpiment, pyrite, mackinawite, carbonate green rust, and siderite.

position is probably related to different structural environments around arsenic. Note that the oxidation state of arsenic in realgar would appear to be +2, but the combination of As–As and As–S bonding in realgar affects the apparent charge of As on a per atom basis. For example, in realgar (As_4S_4), each arsenic atom is bonded to two sulfur atoms and one arsenic atom (Vaughan and Craig, 1978).

XANES spectra of samples obtained from several locations in the HBHA pond are shown in Fig. 9. The absorption maximum for most samples is near 11,870 eV which confirms that arsenic is dominantly present in the +3 oxidation state in the reducing sediments. Samples collected at depths above 1 m show mixed oxidation states with both the +3 and +5 oxidation states of arsenic present. XANES data for magnetic separates provide direct evidence that As(III) is associated with reduced sulfur in NC0901-4b and SC0401-3, specifically with greigite. The As XANES spectra of the magnetic fraction of these sediments compare well with the bulk undifferentiated sample (Fig. 9).

In Fig. 10, XANES data from the reference materials and samples collected in the HBHA pond are compared and related to total sulfur values. Examination of this figure indicates that as sulfur concentrations exceed about 0.5 wt.%, arsenic in the solid phase becomes dominated by the +3 oxidation state. In other words, in sulfate-reducing systems sulfur accumulates in the solid phase and arsenic is effectively reduced. The position of the arsenic absorption edge in the sediments is generally

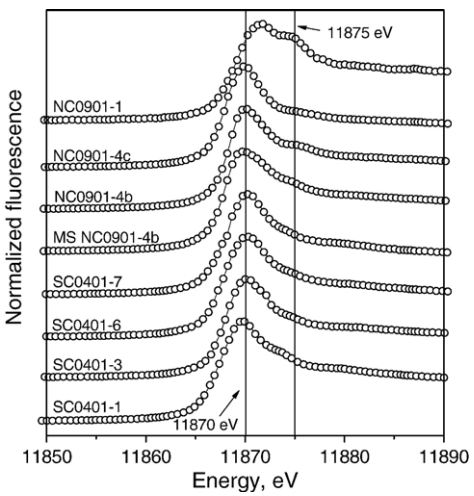

Fig. 9. Arsenic K-edge XANES spectra for sediments from the HBHA pond. Sample MS NC0901-4b is a magnetic separate from NC0901-4b. Sample NC0901-1 was collected at a water depth of 1 m and arsenic in this sample is present in both the +3 and +5 oxidation states.

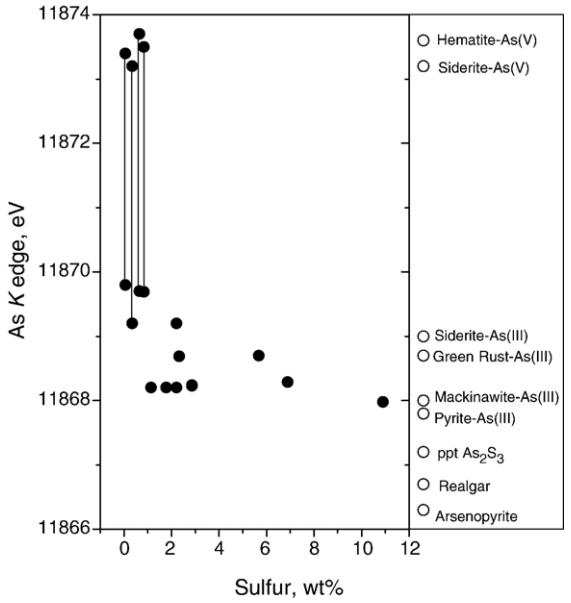

Fig. 10. Arsenic K-edge position from maxima in first derivative curve versus total sulfur concentration in HBHA pond surface sediments. Samples with two local maximums are connected with a line indicating the presence of both As(III) and As(V).

inconsistent with the presence of pure arsenic sulfides (orpiment and realgar) and arsenopyrite. The adsorption edge of samples with >1 wt.% S falls in a range between 11,867.9 to 11,869.5 eV, which compares reasonably well with the range of edge positions of As(III) associated with reference compounds mackinawite, pyrite, carbonate green rust, and siderite, i.e., sulfur- and /or oxygen-coordinated As(III). The concentrations of total arsenic, sulfur, and iron for samples shown in Fig. 10 are presented in Table 2.

In an attempt to more accurately quantify the XANES spectra, we have performed linear combination fitting of reference compound spectra to those of HBHA pond sediments. Results of the least squares fitting are presented in Table 3. Reference compounds used in the fitting analysis were arsenopyrite, precipitated orpiment, mackinawite with As(III), siderite with As(III), and siderite with As(V). In all cases, the dominant components of the sediment spectra were arsenite associated with mackinawite (45% to 96%) and siderite (4% to 79%). Without allowing significant energy shifts of the reference spectra, arsenopyrite could not be fit to any of the sediment spectral data while precipitated orpiment was found to be a minor fractional component, <11%, in some cases (Table 3). The reliability of this estimated fraction of an orpiment-like phase is unknown due to the level of uncertainty associated with XANES linear combination fitting at this concentration.

Table 3
Results of linear combination fitting of XANES spectra of reference compounds to HBHA pond sediments collected from depths below 1 m

Sample	Asp	Orp	Mackinawite, w/As(III)	Siderite, w/As(III)	Siderite, w/As(V)	Sum	Residual
NC0901-1	–	–	–	0.79	0.31	1.10	3.5
SC0401-1	–	0.02	0.54	0.44	–	1.00	1.0
SC0401-6	–	0.02	0.88	0.03	–	0.93	8.0
SC0401-7	–	0.11	0.45	0.49	–	1.05	1.1
SC0401-3	–	0.05	0.85	0.04	–	0.94	5.9
NC0901-4b	–	0.03	0.78	0.12	–	0.93	7.1
NC0901-4c	–	–	0.96	–	–	0.96	8.2

Reference compounds used in the fitting procedure were arsenopyrite (Asp), precipitated orpiment (Orp), mackinawite with As(III), siderite with As (III), and siderite with As(V). Values determined represent the estimated fractional amount of the model compounds that fit individual sample spectra. Ideally the sum of all fractions determined should be equal to 1.00. The residual is an estimate of the goodness of fit.

3.5. Chemical extractions

Chemical extraction methods are useful for providing information about arsenic associations in solid matrices. Numerous previous studies, however, provide evidence that caution must be applied in designing extraction protocols and in interpreting data. In this study, comparatively simple chemical extractions were applied to constrain arsenic solid-phase partitioning and to avoid complications from secondary reactions during chemical extraction. The maximum amount of arsenic associated with pyrite was estimated by assigning the difference between total arsenic (As_T) and As_{HCl} (arsenic leached from oxidized sediments using 1 M HCl) into the measured amount of pyrite on a mass basis. If As_{HCl} was greater than As_T, the amount of arsenic in pyrite is taken to be 0, although this situation occurred in only a few samples. This approach gives maximum arsenic concentrations in pyrite that range from <0.1 to 5.3 wt.%. This estimated arsenic concentration range is certainly within reason based on previous determinations of arsenic in pyrite (e.g., Kolker et al., 1998; Savage et al., 2000). Nonetheless, pyrite can only account for a small percentage, <20%, of the total arsenic budget in reduced sediments of the HBHA pond. Though pyrite is the predicted stable endpoint for reactive iron and sulfur in anoxic sediments, it appears that after a 30 y time period pyrite is a relatively unimportant host for arsenic in the HBHA pond. At the average mass concentration of pyrite in HBHA pond sediments (approx. 1 wt.%), pyrite would need to contain >10 wt.% As in order to be the primary host for arsenic (based upon an average As_T value of 1000 μg g^{-1}).

Several other selective chemical extraction tests were used to probe possible arsenic solid-phase associations and to compliment the XANES results. Traditional sequential extraction procedures (e.g., Tessier et al., 1979; Rauret et al., 1999) were not used in this study because our previous work calls into question the use of these methods for arsenic in sediments containing acid-volatile sulfide (Wilkin and Ford, 2002). In 15 of 17 samples tested, less than 10% of arsenic in the solid-phase was released using 1 M $MgCl_2$ (Fig. 11a). This result suggests that arsenic in the HBHA pond sediments is not readily mobile, but rather is tightly adsorbed to mineral or organic surfaces or arsenic is present within insoluble mineral co-precipitates.

A striking example of an artifact associated with the use of a selective chemical extraction procedure is evident in Fig. 11b. This figure shows the percentage of total arsenic released from redox-preserved, unoxidized sediments using 1 M HCl. Less than about 15% of the total arsenic in sediments is recovered from pristine,

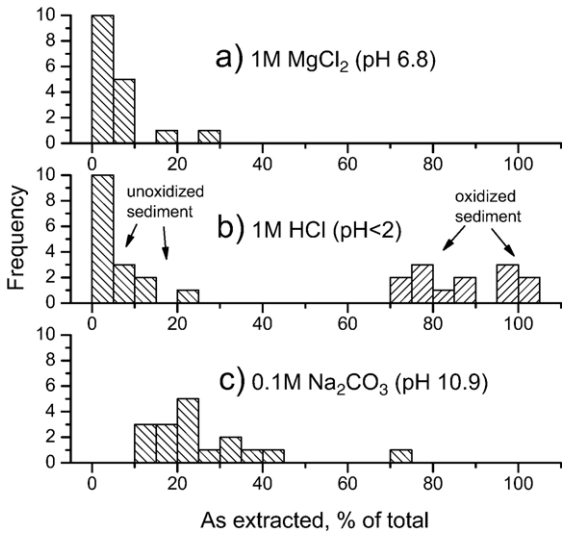

Fig. 11. Histograms showing sample frequency and efficiency of chemical extractions (percent of total arsenic leached) with: a) 1 M $MgCl_2$, b) 1 M HCl (unoxidized versus oxidized sediments), and c) 0.1 M Na_2CO_3.

unoxidized materials. This pattern is caused by the low-pH dissolution of acid-volatile sulfides, release of hydrogen sulfide and arsenic, and consequent low-pH precipitation of As_2S_3 during the extraction procedure (Wilkin and Ford, 2002). During the acidic extraction of unoxidized sediments, arsenic is redistributed to a phase not originally present in the sediments. In the same set of samples that had been oxidized to remove all AVS, a much different pattern with respect to arsenic solubilization is evident. Arsenic is readily leached from oxidized sediments using 1 M HCl. Arsenic is mainly associated with phases soluble in 1 M HCl, which would include mackinawite and greigite in addition to an assortment of other iron-bearing minerals but not orpiment, realgar, arsenian pyrite, or arsenopyrite, a conclusion in good agreement with the spectroscopic results. Note that the treatment used to oxidatively remove AVS was ineffective in destroying CRS (pyrite).

3.6. Theoretical stability of sulfide minerals

Stability relationships between iron sulfides and arsenic sulfides can be evaluated by using equilibrium concepts and thermodynamic data. For example, the competition for solid-phase sulfide between arsenic and iron can be assessed with the following reaction between mackinawite and orpiment:

$$3FeS(s) + 2As(OH)_3^0 + 6H^+ = As_2S_3(s) + 3Fe^{2+} + 6H_2O. \quad (1)$$

In reaction (1), sulfide is conserved in the solids and the reactive aqueous species are arsenite and ferrous iron, consistent with observations from the field site. The logarithm of the equilibrium constant for this reaction is log K=33.89, based on standard state free energies of formation, $\Delta G^o_{f,\,298}$, of disordered orpiment (−76.8 kJ mol^{-1}; Nordstrom and Archer, 2003), mackinawite (−87.7 kJ mol^{-1}; Benning et al., 2000), $As(OH)_3^0$ (−640.0 kJ mol^{-1}; Nordstrom and Archer, 2003), Fe^{2+} (−78.87 kJ mol^{-1}; Wagman et al., 1982), and H_2O(l) (−237.18 kJ mol^{-1}; Wagman et al., 1982).

General inspection of reaction (1) indicates that orpiment formation is favored over mackinawite as concentrations of arsenite increase, as pH decreases, and/or as concentrations of ferrous iron decrease. These relationships are illustrated on an activity–activity–activity diagram for arsenite, ferrous iron, and at pH conditions from 4 to 9 (Fig. 12). At a given pH on Fig. 12, As_2S_3 is predicted to be stable at arsenite activities, ferrous iron activities, and pH values below the plotted plane, whereas FeS is predicted to be stable above the plane. Note that the stability volume of As_2S_3 is encountered with decreasing pH as expected from reaction (1). Furthermore, equilibrium systems at pH 5 would be expected to poise dissolved arsenite concentrations well below EPA's revised drinking water standard of 10 μg l^{-1} at iron concentrations less than about 1 mM. On the other hand, more alkaline systems poised at pH 8 would be expected to yield much higher arsenite concentrations. These trends are reasonable based on the pH-dependent solubility behavior of As_2S_3 observed in laboratory studies (e.g., Eary, 1992). Note that if greigite was used in place of mackinawite on Fig. 12, the iron sulfide stability field at constant pH would expand because greigite is less soluble compared to mackinawite.

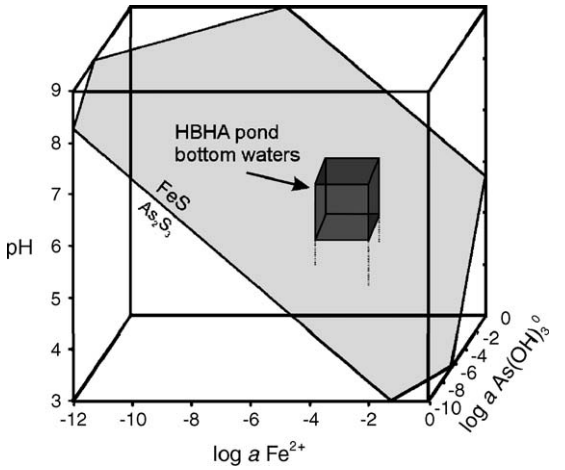

Fig. 12. Activity–activity–activity diagram for arsenite vs. ferrous iron vs. pH (Reaction (1)) showing predominance volumes for FeS and As_2S_3.

The shaded box on Fig. 12 shows the general range of arsenite and ferrous iron activities that have been detected in bottom waters and pore waters of the HBHA pond. The lower concentration range for arsenite is somewhat uncertain due to analytical detection thresholds. The median pH of bottom waters is 7.0±0.4. Field data, when compared to model predictions based on thermodynamic data, suggest that FeS rather than As_2S_3 should dominate solid-phase sulfide, which is consistent with the results of the XANES and selective chemical extraction studies. A general conclusion from Fig. 12 is that As_2S_3 formation is most likely to occur in low-pH systems depleted in reactive iron. Precipitation of FeS will dominate in environments rich in reactive iron, such as the HBHA pond.

In a recent study, Bostick et al. (2004) concluded based primarily on X-ray absorption spectroscopy data that orpiment was a primary host of arsenic in sulfidic

salt marsh sediments near Pescadero (California, USA). Although arsenite and ferrous iron concentrations are not reported in their study, the sediment pore water pH of three samples investigated ranged from about 4.3 to 4.8 (Bostick et al., 2004; their Table 1). Inspection of Fig. 12 indicates that over most reasonable conditions orpiment would in fact be predicted as the primary sulfide encountered near this pH range, except in environments with unusually high ferrous iron activities. In another recent study employing X-ray absorption spectroscopic techniques, O'Day et al. (2004) report the unusual occurrence of realgar in shallow aquifer sediments with no relationship observed between arsenic and iron sulfides. In order to examine the stability relationships among realgar, orpiment, and iron sulfides on a chemical potential diagram such as Fig. 12, the oxidation-reduction potential would need to be constrained or treated as a separate variable, but in general, realgar is be expected to be stable in highly reducing environments depleted in reactive iron. Based on the results of this study and the reports by Bostick et al. (2004) and O'Day et al. (2004), the associations of arsenic in sulfate-reducing systems clearly appear to be wide ranging, complex, and require more study. There is, however, an indication that the striking differences in arsenic behavior may be understandable based on variability in system parameters such as pH, reactive iron abundance, dissolved sulfide concentrations, and arsenic speciation and abundance; it may be fruitful for future studies to use these variables to place findings into context.

Keeping the general goal in mind of minimizing arsenic mobilization and retaining arsenic in the solid phase, reducing (sulfidic) systems at or near equilibrium will be most effective at moderately low pH (4 to 6) and at low concentrations of Fe^{2+}. At this point it is important to emphasize that Fig. 12 or other such model diagrams is based on the assumption that chemical equilibrium is achieved, and, in addition, not all critical reaction processes are considered, e.g., sorption at the mineral–water interface. Although the underlying force to move toward chemical equilibrium is present in natural systems, the equilibrium condition is often not encountered and must be viewed as only one possible endpoint.

4. Summary and conclusions

An understanding of geochemical factors in aquatic systems that govern arsenic cycling between the solid phase and aqueous phase is needed in order to evaluate possible risks to ground-water and surface-water resources. Such geochemical models are needed at contaminated sites, for example, to design long-term monitoring plans, evaluate and select appropriate clean-up technologies, and to prepare contingency plans in the event that prevailing geochemical conditions at a site shift in such a way as to drive mobilization or immobilization of inorganic contaminants like arsenic. In this study, we examined the solid-phase associations of arsenic in organic carbon-rich sediments of a contaminated wetland located adjacent to a hazardous waste site.

Concentrations of arsenic in the wetland sediments range from 20 to 2100 $\mu g\ g^{-1}$ and are highly correlated with concentrations of organic carbon, iron, and sulfur. Solid-phase iron is partitioned into three major forms: pyrite–iron, acid-volatile sulfide–iron, and non-sulfidized reactive-iron. The major forms of sulfur present are pyrite–sulfur and acid-volatile sulfide. Formation of iron monosulfides (mackinawite and greigite) and pyrite begins at or near the sediment–water interface. Maximum concentrations of acid-volatile sulfide and pyrite–sulfur are 8.88 and 3.54 wt.%, respectively. These sulfur concentrations are remarkably high for a freshwater system and are ultimately linked to the presence of ground-water seeps that deliver high concentrations of sulfate, dissolved hydrocarbons, ferrous iron, and arsenic to the wetland. The sediments are also characterized by high concentrations of reactive iron and organic carbon.

The sediments are extensively sulfidized, however, pyrite (FeS_2) was not identified as a primary solid-phase host for arsenic. In fact, pyrite can only account for a small percentage, $<20\%$, of the total arsenic budget in the reduced sediments. This finding is somewhat surprising given the known association between arsenic and pyrite, and is significant with respect to assessing the long-term stability of arsenic in the wetland sediments because pyrite would be a comparatively stable host for arsenic. Although more research is needed, it may be that arsenic incorporation into pyrite is more prevalent in hydrothermal systems as compared to low-temperature sedimentary environments. Indeed, Farquhar et al. (2002) showed that mackinawite may in fact incorporate or sorb considerably more arsenic than pyrite. It is possible that the lack of arsenic associated with pyrite found in this study is related to kinetic factors (i.e., rate of pyritization) that would be important at most hazardous waste sites. Alternatively our results could be related to site-specific variables such as high concentrations of dissolved hydrocarbons or reactive iron that are expected to influence mechanisms of pyrite formation and trace metal incorporation.

For example, it is probable that arsenic speciation (i.e., thioarsenite vs. arsenite species) plays a key role in controlling the extent to which arsenic bonds to pyrite surfaces and accumulates within the pyrite structure during crystal growth. The abundance of reactive iron precludes the formation of thioarsenic species in sulfate-reducing systems by maintaining low dissolved sulfide concentrations (Wilkin et al., 2003). Whereas, environments in which the abundance of reactive iron is limited will favor sulfide accumulation and thioarsenite formation and possibly cause a situation where arsenic accumulation in pyrite or pure arsenic sulfides is favored.

X-ray absorption spectroscopy data for magnetic separates provide direct evidence that As(III) is, at least in part, associated with reduced sulfur in the form of the thiospinel greigite (Fe_3S_4). XANES results demonstrate only the presence of As(III) in the reduced sediments below 1 m depth. The spectroscopic results are consistent with sulfur- and/or oxygen-coordinated As (III) in association with iron monosulfides or other ferrous-bearing carbonates and hydroxides. Arsenic present as arsenopyrite or in pure arsenic sulfide forms (orpiment, realgar) is not indicated to be of any significance in the HBHA pond sediments. XANES results, in combination with selected chemical extraction tests, indicate that arsenic could be mobilized from the sediments through events that drive both oxidation and pH decreases or as a consequence of significant pH increases (pH > 8). Persistence of reducing and near-neutral pH conditions is expected to favor continued sequestration of arsenic in the solid phase in the HBHA pond sediments, partly due to the abundance and continued supply of reactive iron via ground-water inputs.

Acknowledgements

The U. S. Environmental Protection Agency through its Office of Research and Development funded the research described here. It has not been subjected to Agency review and therefore does not necessarily reflect the views of the Agency, and no official endorsement should be inferred. Mention of trade names or commercial products does not constitute endorsement or recommendation for use. The authors greatly appreciate support provided by the staff of the Dow-Northwestern-duPont Collaborative Access Team and the Pacific Northwest Consortium Collaborative Access Team. Use of the Advanced Photon Source is supported by the U. S. Department of Energy, Office of Science, Office of Basic Energy Sciences, under Contract #W-31-109-Eng-38. PNC-CAT facilities at the Advanced Photon Source, and research at these facilities, are supported by the US DOE Office of Science Grant No. DEFG03-97ER45628, the University of Washington, a major facilities access grant from NSERC, Simon Fraser University and the Advanced Photon Source. We also thank J. LeMay (USEPA), C. Su (USEPA), F. Beck (USEPA), P. Clark (USEPA), C. Paul (USEPA), K. Bischoff (East Central University), and N. Xu (Shaw Environmental, Inc.) for field and laboratory support and discussions. Two anonymous journal referees provided constructive comments to help improve the manuscript. **[DR]**

Appendix A

Table A.1 Analytical methods, detection limits, precision and accuracy

Parameter	Method	Detection limit	Precision	Accuracy
Total carbon	Coulometry/combustion	0.01 wt.% C for a 100-mg sample	±3.2% based on 32 analyses of $CaCO_3$	±2.8% using $CaCO_3$ (12.0 wt.% C)
Inorganic carbon	Coulometry/acid extraction	0.01 wt.% C for a 100-mg sample	±2.5% based on 38 analyses of $CaCO_3$	±2.3% using $CaCO_3$ (12.0 wt.% C)
Total sulfur	Coulometry/combustion	0.005 wt.% S for a 100-mg sample	±5.1% based on 35 analyses of NIST 1646a	±2.5% using NIST 1646a (0.35 wt.% S)
AVS	Coulometry/gravimetric hot 1 M HCl extraction	0.005 wt.% S for a 100-mg sample (coulometry)	±10% based on duplicate or triplicate analyses of unknowns	n.d.
CRS	Coulometry/gravimetric hot 1 M Cr(II) extraction	0.005 wt.% S for a 100-mg sample (coulometry)	±4.3% based on 7 analyses of NIST 1646a	n.d.
SO_4–S	Capillary electrophoresis/ alkaline extraction	0.002 wt.% S for a 100-mg sample and 20 mL extraction volume	±3.2% based on 5 analyses of NIST 1646a	n.d.
Metals/metalloids	ICP-OES/microwave assisted digestion/ chemical extraction	1 to 10 ppm for 100-mg sample (depending on element) and 20 mL extraction volume	±5% to 15% based on duplicate or triplicate analyses of unknowns	Variable, depending on element and reference material As (±3% to 12%)

n.d. not determined; standard reference materials used: NIST 1646a Estuary sediment, NIST 2710 Montana soil, NIST 2780 Hard rock mine waste, CCRMP Lake sediment-1.

References

Aggett, J., O'Brien, G.A., 1985. Detailed model for the mobility of arsenic in lacustrine sediments based on measurements in Lake Ohakuri. Environ. Sci. Technol. 19, 231–238.

Atkin, B.P., Somerfield, C., 1994. The determination of total sulphur in geological materials by coulometric titration. Chem. Geol. 111, 131–134.

Belzile, N., Lebel, J., 1986. Capture of arsenic by pyrite in near-shore marine sediments. Chem. Geol. 54, 279–281.

Belzile, N., Tessier, A., 1990. Interactions between arsenic and iron oxyhydroxides in lacustrine sediments. Geochim. Cosmochim. Acta 54, 103–109.

Benning, L.G., Wilkin, R.T., Barnes, H.L., 2000. Reaction pathways in the Fe–S system below 100 °C. Chem. Geol. 164, 25–51.

Berner, R.A., 1980. Early Diagenesis: A Theoretical Approach. Princeton University Press, Princeton, N.J.

Berner, R.A., 1984. Sedimentary pyrite formation: An update. Geochim. Cosmochim. Acta 48, 605–615.

Boesen, C., Postma, D., 1988. Pyrite formation in anoxic environments of the Baltic. Am. J. Sci. 288, 575–603.

Bose, P., Sharma, A., 2002. Role of iron in controlling speciation and mobilization of arsenic in subsurface environment. Water Res. 36, 4916–4926.

Bostick, B.C., Fendorf, S., 2003. Arsenite adsorption on troilite (FeS) and pyrite (FeS_2). Geochim. Cosmochim. Acta 67, 909–921.

Bostick, B.C., Chen, C., Fendorf, S., 2004. Arsenite retention mechanisms within estuarine sediments of Pescadero, CA. Environ. Sci. Technol. 38, 3299–3304.

Brannon, J.M., Patrick, W.H., 1987. Fixation, transformation, and mobilization of arsenic in sediments. Environ. Sci. Technol. 21, 450–459.

Canfield, D.E., 1989. Reactive iron in marine sediments. Geochim. Cosmochim. Acta 53, 619–632.

Canfield, D.E., 2001. Biogeochemistry of sulfur isotopes. In: Valley, J. W., Cole, D.R. (Eds.), Stable Isotope Geochemistry. Mineralogical Society of America, Washington, DC.

Canfield, D.E., Raiswell, R., Westrich, J.T., Reaves, C.M., Berner, R. A., 1986. The use of chromium reduction in the analysis of reduced inorganic sulfur in sediments and shales. Chem. Geol. 54, 149–155.

Chaillou, G., Schäfer, J., Anschutz, P., Lavaux, G., Blanc, G., 2003. The behavior of arsenic in muddy sediments of the Bay of Biscay (France). Geochim. Cosmochim. Acta 67, 2993–3003.

Chambers, L.A., Trudinger, P.A., 1979. Microbiological fractionation of stable sulfur isotopes: a review and critique. Geomicrobiol. J. 1, 249–293.

Chanton, J.P., Martens, C.S., 1985. The effects of heat and stannous chloride addition on the active distillation of acid-volatile sulfide from pyrite-rich marine sediment samples. Biogeochemistry 1, 375–383.

Davis, A., Sellstone, C., Clough, S., Yare, B., 1996. Bioaccumulation of arsenic chromium and lead in fish: constraints imposed by sediment geochemistry. Appl. Geochem. 11, 409–423.

Dellwig, O., Böttcher, M.E., Lipinski, M., Brumsack, H.-J., 2002. Trace metals in Holocene coastal peats and their relation to pyrite formation (NW Germany). Chem. Geol. 182, 423–442.

Eary, L.E., 1992. The solubility of amorphous As_2S_3 from 25 to 90 °C. Geochim. Cosmochim. Acta 56, 2267–2280.

Edenborn, H.M., Belzile, N., Mucci, A., Lebel, J., Silverberg, N., 1986. Observations on the diagenetic behavior of arsenic in a deep coastal sediment. Biogeochemistry 2, 359–376.

Farquhar, M.L., Charnock, J.M., Livens, F.R., Vaughan, D.J., 2002. Mechanisms of arsenic uptake from aqueous solution by interaction with goethite, lepidocrocite, mackinawite, and pyrite: an X-ray absorption spectroscopy study. Environ. Sci. Technol. 36, 1757–1762.

Ford, R.G., Wilkin, R.T., Hernandez, G., 2006. Arsenic cycling within the water column of a small lake receiving contaminated groundwater discharge. Chem. Geol. 228, 137–155. doi:10.1016/j.chemgeo.2005.11.021 (this volume).

Gagnon, C., Mucci, A., Pelletier, E., 1995. Anomalous accumulation of acid-volatile sulphides (AVS) in a coastal marine sediment, Saguenay Fjord, Canada. Geochim. Cosmochim. Acta 59, 2663–2675.

Graham, U.M., Robertson, J.D., 1995. Micro-PIXE analysis of framboidal pyrite and associated maceral types in oil shale. Fuel 74, 530–535.

Harrison, W.J., Pevear, D.R., Lindahl, P.C., 1991. Trace elements in pyrites of the Green River Formation oil shales, Wyoming, Utah, and Colorado. In: Tuttle, M.L., Chap, D. (Eds.), Geochemical, Biochemical, and Sedimentological Studies of the Green River Formation, Wyoming, Utah, and Colorado. USGS Bulletin 1973.

Huerta-Diaz, M.A., Morse, J.W., 1992. Pyritization of trace metals in anoxic marine sediments. Geochim. Cosmochim. Acta 56, 2681–2702.

Huerta-Diaz, M.A., Tessier, A., Carignan, R., 1998. Geochemistry of trace metals associated with reduced sulfur in freshwater sediment. Appl. Geochem. 13, 213–233.

Huffman, E.W.D., 1977. Performance of a new carbon dioxide coulometer. Microchem. J. 22, 567–573.

Hurtgen, M.T., Lyons, T.W., Ingall, E.D., Cruse, A.M., 1999. Anomalous enrichments of iron monosulfide in euxinic marine sediments and the role of H_2S in iron sulfide transformations: examples from Effingham Inlet, Orca Basin, and the Black Sea. Am. J. Sci. 299, 556–588.

Jacobs, L., Emerson, S., Skei, J., 1985. Partitioning and transport of metals across the O_2/H_2S interface in a permanently anoxic basin: Framvaren Fjord, Norway. Geochim. Cosmochim. Acta 49, 1433–1444.

Jones, R.A., Nesbitt, H.W., 2002. XPS evidence for Fe and As oxidation states and electronic states in loellingite ($FeAs_2$). Am. Mineral. 87, 1692–1698.

Jørgensen, B.B., 1982. Mineralization of organic matter in the sea bed—the role of sulphate reduction. Nature 296, 643–645.

Kneebone, P.E., Hering, J.G., 2000. Behavior of arsenic and other redox-sensitive elements in Crowley Lake, CA: a reservoir in the Los Angeles aqueduct system. Environ. Sci. Technol. 34, 4307–4312.

Kolker, A., Cannon, W.F., Westjohn, D.B., Woodruff, L.G., 1998. Arsenic-rich pyrite in the Mississippian Marshall sandstone: source of anomalous arsenic in southeastern Michigan ground water. Geological Society of America Annual Meeting, Programs and Abstracts, vol. 30, p. 59.

Kornicker, W.A., Morse, J.W., 1991. Interactions of divalent cations with the surfaces of pyrite. Geochim. Cosmochim. Acta 55, 2159–2171.

La Force, M.J., Hansel, C.M., Fendorf, S., 2000. Arsenic speciation, seasonal transformations, and co-distribution with iron in a mine waste-influenced palustrine emergent wetland. Environ. Sci. Technol. 34, 3937–3943.

Lennie, A.R., Redfern, S.A.T., Champness, P.E., Stoddart, C.P., Schofield, P.F., Vaughan, D.J., 1997. Transformation of mackinawite to greigite: an in situ X-ray powder diffraction and

transmission electron microscope study. Am. Mineral. 82, 302–309.
Li, Y.-H., Gregory, S., 1974. Diffusion of ions in sea water and in deep-sea sediments. Geochim. Cosmochim. Acta 38, 703–714.
Loring, D.H., Dahle, S., Naes, K., Dos Santos, J., Skei, J.M., Matishov, G.G., 1998. Arsenic and other trace metals in sediments from the Kara Sea and the Ob and Yenisey Estuaries, Russia. Aquat. Geochem. 4, 233–252.
McCready, R.G.Z., 1975. Sulphur isotope fractionation by Desulfovibrio and Desulfotomaculum. Geochim. Cosmochim. Acta 39, 1395–1401.
Middelburg, J.J., 1991. Organic carbon, sulphur, and iron in recent semi-euxinic sediments of Kau Bay, Indonesia. Geochim. Cosmochim. Acta 55, 815–828.
Moore, J.N., Ficklin, W.H., Johns, C., 1988. Partitioning of arsenic and metals in reducing sulfidic sediments. Environ. Sci. Technol. 22, 432–437.
Morse, J.W., 1994. Interactions of trace metals with authigenic sulfide minerals: implications for their bioavailability. Mar. Chem. 46, 1–6.
Morse, J.W., 1999. Sulfides in sandy sediments: new insights on the reactions responsible for sedimentary pyrite formation. Aquat. Geochem. 5, 75–85.
Mucci, A., Richard, L.-F., Lucotte, M., Guignard, C., 2000. The differential geochemical behavior of arsenic and phosphorus in the water column and sediments of the Saguenay Fjord Estuary, Canada. Aquat. Geochem. 6, 293–324.
Nicholas, D.R., Ramamoorthy, S., Palace, V., Spring, S., Moore, J.N., Rosenzweig, F., 2003. Biogeochemical transformations of arsenic in circumneutral freshwater sediments. Biodegradation 14, 123–137.
Nordstrom, D.K., Archer, D.G., 2003. Arsenic thermodynamic data and environmental geochemistry. In: Welch, A.H, Stollenwerk, K. G. (Eds.), Arsenic in Ground Water. Kluwer Academic Publishers, Boston, MA, pp. 1–25.
O'Day, P.A., Vlassopoulos, D., Root, R., Rivera, N., 2004. The influence of sulfur and iron on dissolved on dissolved arsenic concentrations in the shallow subsurface under changing redox conditions. Proc. Natl. Acad. Sci. 101, 13703–13708.
Ostwald, J., England, B.M., 1979. The relationship between euhedral and framboidal pyrite in base-metal sulfide ores. Mineral. Mag. 43, 297–300.
Peterson, M.L., Carpenter, R., 1983. Biogeochemical processes affecting total and arsenic species distributions in an intermittently anoxic fjord. Mar. Chem. 12, 295–321.
Pierce, M.L., Moore, C.B., 1982. Adsorption of arsenite and arsenate on amorphous iron hydroxide. Water Res. 16, 1247–1253.
Rauret, G., López-Sánchez, J.F., Sahuquillo, A., Rubio, R., Davidson, C., Ure, A., Quevauviller, Ph., 1999. Improvement of the BCR three step sequential extraction procedure prior to the certification of new sediment and soil reference materials. J. Environ. Monit. 1, 57–61.
Raiswell, R., Plant, J., 1980. The incorporation of trace elements into pyrite during diagenesis of black shales, Yorkshire, England. Econ. Geol. 75, 684–689.
Ressler, T., 1998. WinXAS: a program for X-ray absorption spectroscopy data analysis under MS-Windows. J. Synchrotron Radiat. 5, 118–122.
Rickard, D., Schoonen, M.A.A., Luther III, G.W., 1995. Chemistry of iron sulfides in sedimentary environments. Geochemical Transformations of Sedimentary Sulfides. American Chemical Society Symposium Series, vol. 612. American Chemical Society, Washington, DC, pp. 168–193 (Chapter 9).
Rickard, D., Butler, I.B., Oldroyd, A., 2001. A novel iron sulphide mineral switch and its implications for earth and planetary science. Earth Planet. Sci. Lett. 189, 85–91.
Riedel, G.F., Sanders, J.G., Osman, R.W., 1987. The effect of biological and physical disturbances on the transport of arsenic from contaminated estuarine sediments. Estuar. Coast. Shelf Sci. 25, 693–706.
Ronen, D., Magaritz, M., Levy, I., 1987. An in situ multilevel sampler for preventive monitoring and study of hydrochemical profiles in aquifers. Ground Water Monit. Rev. 7, 69–74.
Saulnier, I., Mucci, A., 2000. Trace metal remobilization following the resuspension of estuarine sediments: Saguenay Fjord, Canada. Appl. Geochem. 15, 203–222.
Saunders, J.A., Pritchett, M.A., Cook, R.B., 1997. Geochemistry of biogenic pyrite and ferromanganese stream coatings: a bacterial connection? Geomicrobiol. J. 14, 203–217.
Savage, K.S., Tingle, T.N., O'Day, P.A., Waychunas, G.A., Bird, D.K., 2000. Arsenic speciation in pyrite and secondary weathering phases, Mother Lode Gold District, Tuolumne County, California. Appl. Geochem. 15, 1219–1244.
Schoonen, M.A.A., Barnes, H.L., 1991. Reactions forming pyrite and marcasite from solution: II. Via FeS precursors below 100 °C. Geochim. Cosmochim. Acta 55, 1505–1514.
Simon, G., Huang, H., Penner-Hahn, J.E., Kesler, S.E., Kao, L.-S., 1999. Oxidation state of gold and arsenic in gold-bearing arsenian pyrite. Am. Mineral. 84, 1071–1079.
Su, C., Wilkin, R.T., 2005. Arsenate and arsenite sorption on and arsenite oxidation by iron (II, III) hydroxycarbonate green rust. In: O'Day, P., Vlassopoulos, D., Meng, X., Benning, L. (Eds.), Advances in Arsenic Research: Integration of Experimental and Observational Studies and Implications for Mitigation, ACS Symposium Series, vol. 915. American Chemical Society, Washington, DC, pp. 25–40 (Chapter 3).
Sullivan, K.A., Aller, R.C., 1996. Diagenetic cycling of arsenic in Amazon shelf sediments. Geochim. Cosmochim. Acta 55, 1465–1477.
Tessier, A., Campbell, P.G.C., Bison, M., 1979. Sequential extraction procedure for the speciation of particulate trace metals. Anal. Chem. 51, 844–851.
Tuttle, M.L., Goldhaber, M.B., Williamson, D.L., 1986. An analytical scheme for determining forms of sulphur in oil shales and associated rocks. Talanta 33, 953–961.
Vaughan, D.J., Craig, J.R., 1978. Mineral Chemistry of Metal Sulfides. Cambridge University Press, Cambridge.
Vavelidis, M., 1995. Framboidal pyrite from the Kuroko-type barite mineralization of the Katsimouti Area, Milos Island, Greece. Chem. Erde 55, 281–294.
Wagman, D.D., Evans, W.H., Parker, V.B., Schumm, R.H., Halow, I., Bailey, S.M., Churney, K.L., Nuttall, R.L., 1982. The NBS tables of chemical thermodynamic properties. J. Phys. Chem. Ref. Data 11, 1–392.
Wick, L.Y., Gschwend, P.M., 1998. Source and chemodynamic behavior of diphenyl sulfone and *ortho*- and *para*-hydroxybiphenyl in a small lake receiving discharges from an adjacent Superfund site. Environ. Sci. Technol. 32, 1319–1328.
Wick, L.Y., McNeill, K., Rojo, M., Medilanski, E., Gschwend, P.M., 2000. Fate of benzene in a stratified lake receiving contaminated groundwater discharges from a Superfund site. Environ. Sci. Technol. 34, 4354–4362.

Widerlund, A., Ingri, J., 1995. Early diagenesis of arsenic in sediments of the Kalix River estuary, northern Sweden. Chem. Geol. 125, 185–196.

Wilkin, R.T., Barnes, H.L., 1996. Pyrite formation by reactions of iron monosulfides with dissolved inorganic and organic sulfur species. Geochim. Cosmochim. Acta 60, 4167–4179.

Wilkin, R.T., Ford, R.G., 2002. Use of hydrochloric acid for determining solid-phase arsenic partitioning in sulfidic sediments. Environ. Sci. Technol. 36, 4921–4927.

Wilkin, R.T., Wallschlaeger, D., Ford, R.G., 2003. Speciation of arsenic in sulfidic waters. Geochem. Trans. 4, 1–7.

Wolthers, M., Charlet, L., van der Weijden, H., van der Linde, P., Rickard, D., 2005a. Arsenic mobility in the ambient sulfidic environment: sorption of arsenic(V) and arsenic(III) onto disordered mackinawite. Geochim. Cosmochim. Acta 69, 3482–3492.

Wolthers, M., Butler, I.B., Rickard, D., Mason, P.R.D., 2005b. Arsenic incorporation into p rite at ambient environmental conditions: a continous-flow experiment. In: O'Day, P., Vlassopoulos, D., Meng, X., Benning, L. (Eds.), Advances in Arsenic Research: Integration of Experimental and Observational Studies and Implications for Mitigation, ACS Symposium Series, vol. 915. American Chemical Society, Washington, DC, pp. 60–76 (Chapter 5).